

Enhancement of thermal rectification by asymmetry engineering of thermal conductivity and geometric structure for multi-segment thermal rectifier

Fu-Ye Du(杜甫烨), Wang Zhang(张望), Hui-Qiong Wang(王惠琼), and Jin-Cheng Zheng(郑金成)
Citation: Chin. Phys. B, 2023, 32 (**6**): 064402. DOI: 10.1088/1674-1056/acc78c
Journal homepage: http://cpb.iphy.ac.cn; http://iopscience.iop.org/cpb

What follows is a list of articles you may be interested in

An optimized smearing scheming for first Brillouin zone sampling and its application on thermal conductivity prediction of graphite

Chengye Li(李承业), Changying Zhao(赵长颖), and Xiaokun Gu(顾骁坤)
Chin. Phys. B, 2023, 32 (**6**): 064401. DOI: 10.1088/1674-1056/ac9223

Thermal transport properties of two-dimensional boron dichalcogenides from a first-principles and machine learning approach

Zhanjun Qiu(邱占均), Yanxiao Hu(胡晏箫), Ding Li(李顶), Tao Hu(胡涛), Hong Xiao(肖红),Chunbao Feng(冯春宝), and Dengfeng Li(李登峰)
Chin. Phys. B, 2023, 32 (**5**): 054402. DOI: 10.1088/1674-1056/acb9e6

Modeling of thermal conductivity for disordered carbon nanotube networks

Hao Yin(殷浩), Zhiguo Liu(刘治国), and Juekuan Yang(杨决宽)
Chin. Phys. B, 2023, 32 (**4**): 044401. DOI: 10.1088/1674-1056/acb0be

Accurate prediction of the critical heat flux for pool boiling on the heater substrate

Fengxun Hai(海丰勋), Wei Zhu(祝薇), Xiaoyi Yang(杨晓奕), and Yuan Deng(邓元)
Chin. Phys. B, 2022, 31 (**6**): 064401. DOI: 10.1088/1674-1056/ac523c

Construction and mechanism analysis on nanoscale thermal cloak by *in-situ* annealing silicon carbide film

Jian Zhang(张健), Hao-Chun Zhang(张昊春), Zi-Liang Huang(黄子亮), Wen-Bo Sun(孙文博), and Yi-Yi Li(李依依)
Chin. Phys. B, 2022, 31 (**1**): 014402. DOI: 10.1088/1674-1056/ac2809

SPECIAL TOPIC — Celebrating the 100th Anniversary of Physics Discipline of Xiamen University

Enhancement of thermal rectification by asymmetry engineering of thermal conductivity and geometric structure for multi-segment thermal rectifier

Fu-Ye Du(杜甫烨)[1], Wang Zhang(张望)[1], Hui-Qiong Wang(王惠琼)[1,2], and Jin-Cheng Zheng(郑金成)[1,2,†]

[1] *Department of Physics, Xiamen University, Xiamen* 361005, *China*
[2] *Department of Physics, Xiamen University Malaysia*, 439000 *Sepang, Selangor, Malaysia*

(Received 13 December 2022; revised manuscript received 17 February 2023; accepted manuscript online 25 March 2023)

Thermal rectification is an exotic thermal transport phenomenon, an analog to electrical rectification, in which heat flux along one direction is larger than that in the other direction and is of significant interest in electronic device applications. However, achieving high thermal rectification efficiency or rectification ratio is still a scientific challenge. In this work, we performed a systematic simulation of thermal rectification by considering both efforts of thermal conductivity asymmetry and geometrical asymmetry in a multi-segment thermal rectifier. It is found that the high asymmetry of thermal conductivity and the asymmetry of the geometric structure of multi-segment thermal rectifiers can significantly enhance the thermal rectification, and the combination of both thermal conductivity asymmetry and geometrical asymmetry can further improve thermal rectification efficiency. This work suggests a possible way for improving thermal rectification devices by asymmetry engineering.

Keywords: thermal conductivity, simulation, thermal rectification, multi-segment thermal rectifier

PACS: 44.10.+i, 66.30.Xj, 66.70.−f **DOI:** 10.1088/1674-1056/acc78c

1. Introduction

The heat conduction of the contact surface formed by two different solid materials contacting each other can be direction-dependent (the heat transfers in one direction much faster than in the other), which is called the thermal rectification phenomenon. The thermal rectification can be realized in many different ways, such as different temperature-dependent thermal conductivities between two materials,[1–8] asymmetric electron transport,[9,10] interface thermal barrier,[11–13] roughness, and flatness in surface contact,[14–16] strain warping between two solids,[17–23] asymmetry of nanostructures,[4,24,25] non-uniform mass,[26–28] anharmonic/nonlinear lattices,[29–36] and composite metamaterials.[37]

As early as in 1936, a solid state rectifier using copper oxide has been proposed.[10] After that, the research activities on thermal rectification have been increased. Thermal devices based on thermal rectification have received lots of interest and attentions in recent years due to their pivotal role in heat dissipation, especially in the field of electronic equipment. As the size of electronic devices gets smaller and smaller, the heat dissipation by thermal management devices or low-dimensional thermal transport will become a more and more important direction of future development.[39–46] Heat flow control is also very meaningful in many other fields,[47] such as aerospace,[48] refrigeration,[49,50] biology, chemistry, and pharmacy,[51–53] buildings,[54–56] and so on.

In the past studies of thermal rectification materials and devices, how to obtain higher thermal rectification has been explored. This has led to a variety of experimental and theoretical advances, including attempts at creating novel structures and materials to improve thermal management capabilities.[42] For example, Peyrard reported a design of thermal rectifier;[35] Li *et al.* proposed thermal rectifiers by coupling two nonlinear lattices,[30] and utilizing carbon nanotubes by molecular dynamics simulations.[57] Many studies had also been reported on the theoretical simulation of thermal logic circuits.[26,38,58,59] In terms of experiments, Chang *et al.* reported a solid-state thermal rectifier based on carbon nanotubes through uneven mass distribution.[27] A two-segment oxide rectifier successfully achieved a thermal rectification of 1.43.[1] The triangular thermal rectifier of multi-layer reduced graphene oxide by Tian *et al.* obtained a rectification of 1.21.[60] Nevertheless, there remains a lot of work to be done to improve the thermal rectification efficiency being closer to the theoretical limit. Approaches on thermal rectification can be roughly classified into two aspects: one is based on the difference of thermal conductivity and the other is the difference of geometric structure. However, much less study has been reported for combing the two aforementioned aspects. Very recently, it was shown that the thermoelectric transport is strongly associated with the asymmetry of electron transport density function.[61] It would be interesting to see how the

†Corresponding author. E-mail: jczheng@xmu.edu.cn

© 2023 Chinese Physical Society and IOP Publishing Ltd

asymmetries of thermal conductivity or structure or the combination of both affect the thermal rectification.

This paper systematically describes how to achieve higher thermal rectification by engineering asymmetry in thermal conductivity or in geometric structure. We also point out that the thermal rectification can be even further enhanced by combining both asymmetry of thermal conductivity and that of geometric structure. Our work is mainly divided into three parts: the influence of thermal conductivity optimization on thermal rectification, the influence of geometric structure optimization on thermal rectification, and whether the combination of the two can further optimize thermal rectification. Based on the simulation and verification of oxide rectifiers,[1,60] various different multi-segment models are constructed to explore the further optimization of thermal rectification by geometric structure and thermal conductivity.

2. Methods and models

The simulation program, Energy2D, is an open-source interactive code based on computational physics with accurate simulation of heat transfer — conduction, convection, and radiation, and their coupling with particle dynamics. Using Energy2D,[62] we simulated some models in two dimensions according to

$$\rho c[\partial T/\partial t + \nabla(\boldsymbol{v}t)] = \nabla(k\nabla T) + \dot{Q}, \tag{1}$$

where ρ denotes the density of the material, c denotes the specific heat capacity of the material, $\boldsymbol{v}$ denotes the velocity field describing convective heat dissipation, and $\dot{Q}$ is the internal heat generation. The heat equation, *i.e.*, Eq. (1), can be solved using a finite-difference time-domain (FDTD) method in both space and time domains. Energy2D has been widely used in heat transfer simulation in various materials and systems, demonstrating its wide applications across science and engineering.[62]

General multi-segment rectifier models, which are close to many experimental setup of solid state thermal rectifier, are used in our simulation. Figure 1 shows a typical model diagram of a multi-segment thermal rectifier that we designed, which consists of multiple rectangle grids (building blocks). Thermometers and heat flow meters (heat flux sensor) are placed in the first grid. We use the constant temperature source using the Dirichilet boundary condition to simulate the cold end and the power source to provide the heat and to simulate the hot end (heater). Heat flow is controlled by adjusting the power density in the power source. The proposed model is designed to be as closer to experimental devices as possible, thus can be conveniently realized in experiments but at the same time remains flexible for proof-of-concept engineering.

The heat current density J in the multi-segment thermal rectifiers is described by Fourier's law[1,33]

$$J = -k[x, T(x)]\frac{\mathrm{d}T(x)}{\mathrm{d}x}, \tag{2}$$

where $k[x, T(x)]$ denotes the thermal conductivity as a function of spatial position x and temperature T. The rectifying coefficient R is thus defined by the ratio of forward and reverse heat current density,[1,33]

$$R = \frac{|J_\mathrm{f}|}{|J_\mathrm{r}|}. \tag{3}$$

Alternatively, one can also use the ratio of thermal power P_f and P_r,[60]

$$R = \frac{|P_\mathrm{f}|}{|P_\mathrm{r}|}. \tag{4}$$

In our testing, as will be shown later in multi-segment thermal rectifier with fixed temperature difference at the two ends, ΔT, the ratio of forward and reverse heat current density is equivalently to the ratio of thermal power P_f and P_r for the case of uniform shape. For thermal rectifier with geometric asymmetry, we will use Eq. (4) only, because the heat flux is too sensitive to the location of heat flux sensor. The thermal rectification obtained by the ratio of thermal power will be more robust.

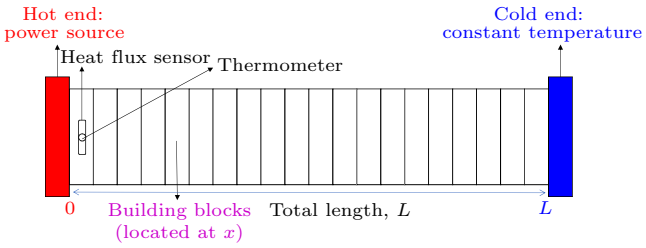


Fig. 1. Conceptual diagram of the multi-segment thermal rectification model.

3. Results and discussion

3.1. Effects of thermal conductivity on thermal rectification

3.1.1. Verification of simulation comparing with experiments

Figure 2 shows the typical theoretical model to simulate experimental thermal rectification device.[1] The setup of the model was adjusted according to the specific conditions of the experiment. We use a multi-segment model to simulate materials with temperature-dependent thermal conductivity. Experimentally, the two segments of material are divided into multiple sections (building blocks) in the theoretical multi-segment model; in such way, the thermal conductivity at the corresponding temperature can be precisely assigned to the corresponding building blocks. Taking experimental

two-segment thermal rectifier device (made by $LaCoO_3$ (LCO) and $La_{0.7}Sr_{0.3}CoO_3$ (LSCO) segments)[1] as an example, each of the LCO and LSCO segments is divided into six building blocks, and the actual sizes of the experimental device are adapted in our simulation. The size of each two-dimensional (2D) rectangle building block is 1.2-mm wide and the thickness is 1 mm. The upper end is connected to the power density to simulate the hot end, and the lower end is connected to the heat sink with constant temperature (40 K, the same as the temperature setup in the experiment[1]). The power density at the hot end is adjusted to be as closer to the experimental condition as possible. Four thermometers are placed at a distance of 5 mm from the endpoints of the two oxide materials, which is similar with the experimental setup.[1] The LCO oxide material is not only showing unusual temperature-dependent spin-state transition,[63] but also exhibiting quite different thermal conductivity with the LSCO alloy (Fig. 2(b)). The large difference between the temperature-dependent thermal conductivity of LCO and that of LSCO boosts the large thermal rectification effect in the LCO–LSCO two-segment thermal rectifier. Such a typical thermal rectifier can be used for the verification of simulation comparing with experiments.

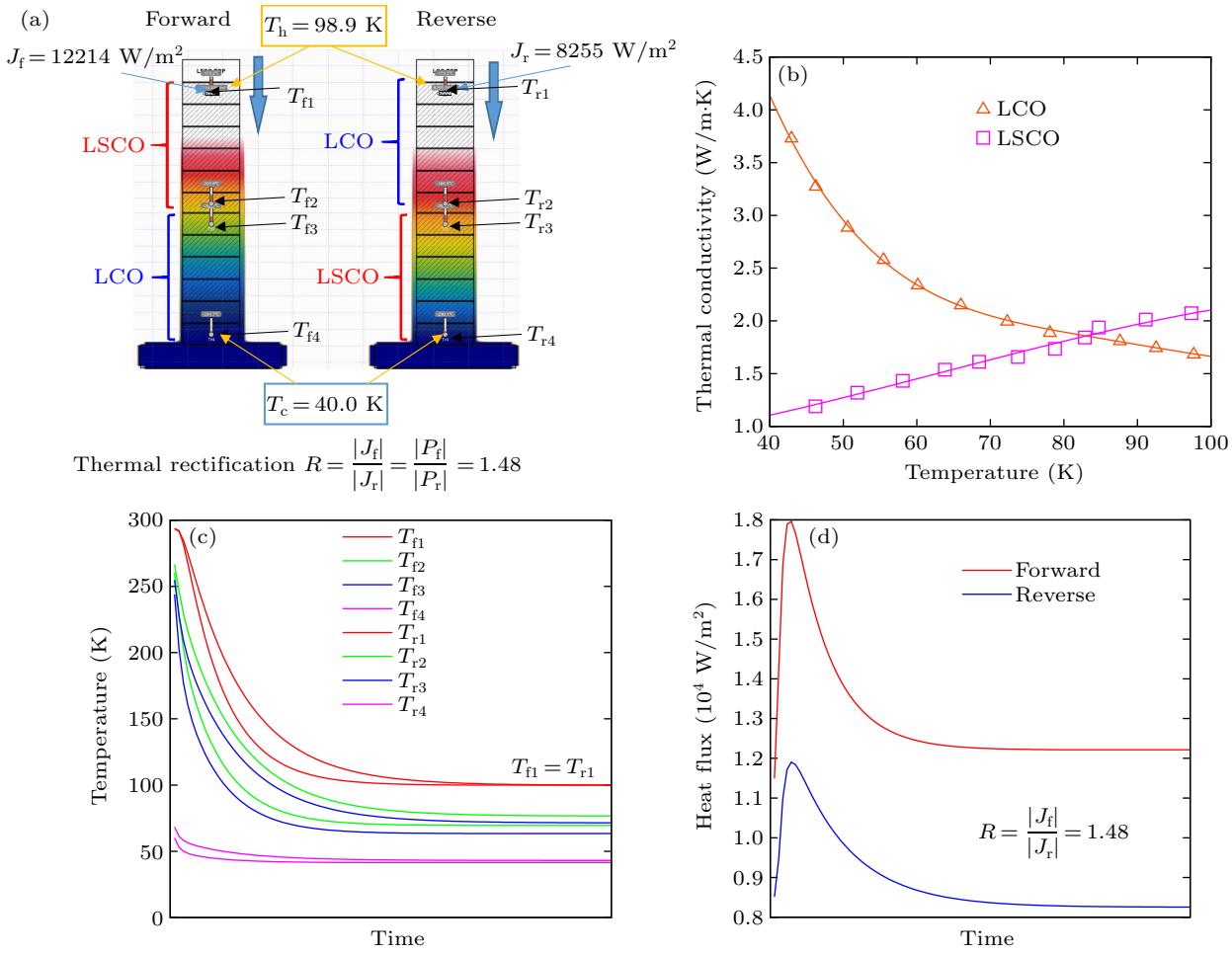


Fig. 2. Experimental two-segment thermal rectification device ($LaCoO_3$ and $La_{0.7}Sr_{0.3}CoO_3$ segments) represented by the theoretical multi-segment thermal rectification model in simulation. (a) Multi-segment thermal rectification model. For the model on the left-hand side, the top half part is made of $La_{0.7}Sr_{0.3}CoO_3$, and the bottom half part is $LaCoO_3$. For the model on the right-hand side, the setup is in the opposite direction, *i.e.* the top half part is $LaCoO_3$, while the bottom half part is $La_{0.7}Sr_{0.3}CoO_3$. The rainbow color represents the temperature distribution in the steady state (40 K–98.9 K). The cold end is heat sink at the temperature of 40 K, and the hot end is heated by power source and reaches 98.9 K when the system is steady. (b) The thermal conductivity of $LaCoO_3$ and $La_{0.7}Sr_{0.3}CoO_3$ as a function of temperature. (c) The temperature profile of different parts of multi-segment thermal rectifier as a function of time (it reaches the steady state when $T_{f1} = T_{r1}$). (d) The heat flux as a function of time. The rectification can be obtained by $R = |J_f|/|J_r| = |P_f|/|P_r| = 1.48$, which is in good agreement with the experimental value of 1.43.

As shown in Fig. 2(c), the steady-state temperatures of the top thermometer for both forward and reverse configurations reach about 100 K by adjusting the power density in the power source and then the thermal rectification is verified at this temperature. The thermal rectification obtained by simulation is 1.48 using the ratio of forward and reverse heat flux (Eq. (3)), and shown in Fig. 2(d)) or the ratio of power density at power source for the forward and reverse configurations (Eq. (4)), which is very close to the value of 1.43 obtained by the experiment.[1] The very good agreement of thermal rectification between simulation and experimental measurement demonstrates the excellent capability of our approach to perform thermal rectification simulations. We thus will apply the similar method to perform systematic simulation of thermal

rectification by considering both efforts of thermal conductivity asymmetry and geometrical asymmetry in a multi-segment thermal rectifier, and to design multi-segment thermal rectifier with novel structures combining both thermal conductivity asymmetry and geometrical asymmetry.

3.1.2. Enhancement of thermal rectification by modifying thermal conductivity

The asymmetry of electron transport density function, namely, the thermoelectric skewness, is the key to enhance thermoelectric power.[61] Interestingly, the temperature-dependent asymmetry of thermal conductivity is also an important factor that affects the thermal rectification.[64] Therefore, we can further improve thermal rectification by modifying the thermal conductivity asymmetry of the material of two segments. We tried the method by modifying the thermal conductivity of the two materials as a function of temperature and to explore whether the thermal rectification would be improved.

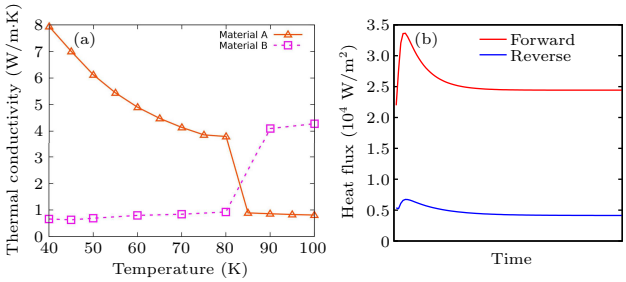


Fig. 3. Multi-stage thermal rectification model with modified thermal conductivities. (a) Modified thermal conductivity of materials A and B as a function of temperature. (b) Resulting heat flux of thermal rectifier in the forward and reverse directions as a function of time. The thermal conductivity is increased in the lower temperature part of material A and the high temperature region of material B, while the thermal conductivity is reduced for the high temperature part of A and the low temperature part of B, compared with original samples in Fig. 2. The other parameters including the two-segment configurations are similar to those in Fig. 2. The rectification is $R = |J_f|/|J_r| = |P_f|/|P_r| = 5.91$.

We found that if we doubled the difference of the thermal conductivity of materials in bi-segment rectifier (for example, the aforementioned LCO–LSCO rectifier model) from before to after the crossover point (shown in Fig. 3(a)), the thermal rectification of the updated rectifier device would be increased by almost 4 times ($R = |J_f|/|J_r| = |P_f|/|P_r| = 5.91$). Here we can use the formula of thermal conductivity and heat current density (Eq. (2)) to explain the origin of enhancement of thermal rectification. It can be seen from the formula that the thermal conductivity at the forward direction increases twice but that along the reverse direction reduces twice, thus it results in four times difference of heat flux (Fig. 3(b)), and it will lead to the significant four times enhancement of thermal rectification. Although we should note that such modification of thermal conductivity is arbitrary, it is good enough to show that the sensitivity of thermal rectification to thermal conductivity changes. Our simulations clearly demonstrate that the thermal rectification is strongly correlated with the difference of temperature-dependent thermal conductivity of materials A and B in bi-segment rectifier. One can select realistic materials with largely different temperature-dependent thermal conductivities for designing better bi-segment rectifier.

3.2. Geometric effects on thermal rectification

3.2.1. Shape effects of the segments

Model 1. The two-rectangular shaped solid-state thermal rectifier based on reduced graphene oxide

It has been reported that the asymmetry of the geometric structure will cause thermal rectification in many studies. Here we propose two ways to enhance thermal rectification through geometric design, namely external shape effects, and geometric internal asymmetry. In order to compare with experimental results,[60] we adapted a typical bi-segment thermal rectifier with different shapes of segments to perform numerical simulations. The two-rectangular shaped solid-state thermal rectifier model based on reduced graphene oxide is used for simulation.

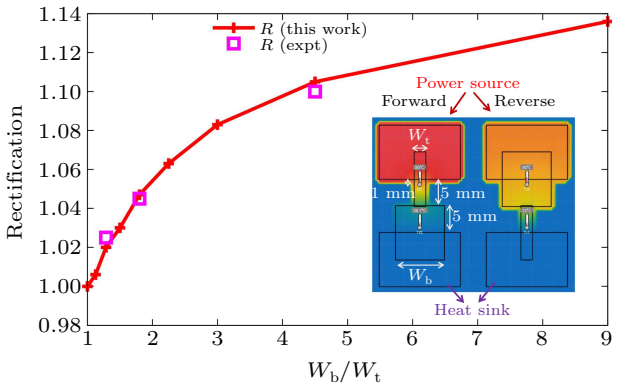


Fig. 4. The bi-segment thermal rectifier model based on the reduced graphene oxide with an asymmetric rectangular shape. Inset, for the left-hand side forward model, the hot end is on the top, the cold end is located at the bottom, and *vice versa* for the right-hand side reverse model. Each segment is 10-mm thick, and the thermometers and heat flow sensors are placed 1 mm from the heat end and the cold end. The curve shows the thermal rectification as a function of W_b/W_t, the width ratio of bottom segment and top segment. The thermal conductivity of the reduced graphene oxide is used in the simulation.

Firstly, we used the geometric parameters from experiment[60] to verify our multi-segment thermal rectifier model based on reduced graphene oxide (rGO) with asymmetric shape. As shown in Fig. 4 (insert picture), we used a constant temperature source (heat sink) to simulate the cold end and a power source to simulate the hot end. The model is divided into two rectangular sections, and the thickness of each section is 10 mm. The thermometers and heat flow sensors are placed 1 mm from the heat end. The thermal rectification given in the experiment[60] is defined as the ratio of forward and reverse thermal powers (Eq. (4)), which can be calculated by the power density in the power source at the heat end. Taking a typical setting in the experiment as an exam-

ple, we used the same geometrical parameters from the reported experiment[60] for our simulation. That is, the ratio of the lower segment (W_b) to the upper segment (W_t) is W_b/W_t (namely, the width of the upper rectangle is set to W_t, the width of the lower rectangle is set to W_b), and the power density is adjusted to control the temperature so that T_{f1} is equal to T_{r2}, with the temperature difference between the hot end and the cold end being 30 K.

As a result, the rectification for rGO thermal rectifier with the setting of $W_b = 9$ mm and $W_t = 2$ mm obtained from the simulation is 1.105, which is in excellent agreement with the experimental value (1.10).[60] The thermal rectifications for other W_b/W_t cases are also very close to experimental data, as shown in Fig. 4. These simulations indicate the amazing capability of our model representing the realistic thermal rectifier. Therefore, our models can be further used to optimize the design of multi-segment thermal rectifier, not only by choosing the suitable materials with optimal thermal conductivity, but also by adjusting the geometric shapes.

Model 2. The Proposed multi-segment size gradient (MSSG) thermal rectifier

In the previous section, we already demonstrated that our bi-segment model can well reproduce the experimental rectification based on reduced graphene oxide. It is worth noting that the reduced graphene oxide has a high thermal conductivity. To extend our multi-segment model to a more general case, and to emphasize the effects of shapes, we will later set the thermal conductivity in all parts of rectifier to be as simple as unit, that is, 1 W/(m·K), to show how to further enhance the rectification by shape design.

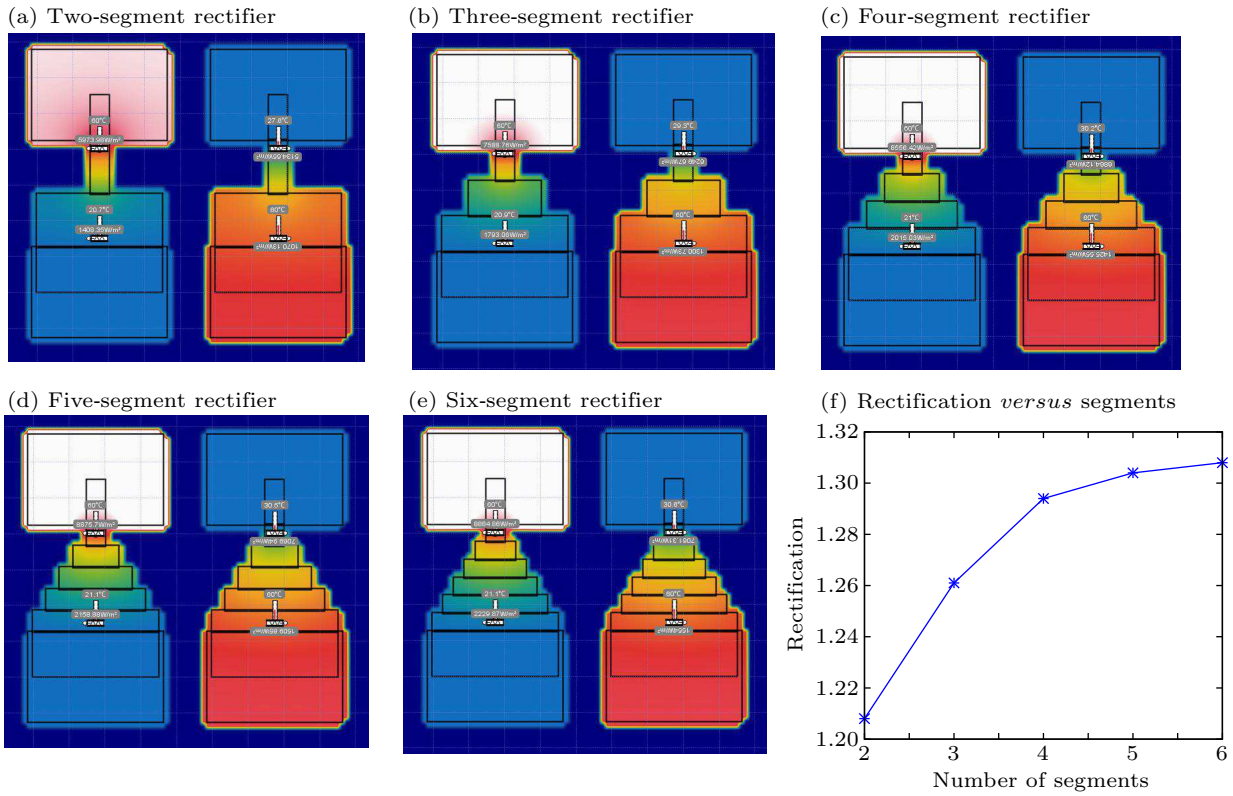


Fig. 5. Proposed multi-segment size gradient (MSSG) thermal rectifier: (a)–(e) models with different numbers of gradient segments. (f) Rectification as a function of number of segments. The width of the uppermost rectangle is 2 mm and the width of the lowest rectangle is 14 mm. The other segments in the middle region are designed with gradient width.

We now will modify the bi-segment thermal rectifier to multi-segment size gradient (MSSG) thermal rectifier with the increase number of layers or segments with a gradient width in the thermal rectifier but keeping the same total length. This is to further explore the relationship between the thermal rectification and the number of rectangles due to asymmetric geometry. As shown in Figs. 5(a)–5(e), we design a series of more general multi-segment thermal rectifier models with a fixed total length (12 mm) but with different numbers of segments or layers with a gradient width. The ratio of the top-layer width and the bottom-layer width is set to be 2:14. Namely, the width of the uppermost rectangle is 2 mm and the width of the lowest rectangle is 14 mm (the distance between the top and bottom sides of the rectangle is defined as the length, and the distance between the left and right sides is defined as the width). Other settings are similar to the bi-segment thermal rectifier as shown in Fig. 4.

Different from the bi-segment thermal rectifier, our newly proposed MSSG thermal rectifier can further enhance the rectification significantly, as shown in Fig. 5(f). It can be seen that the thermal rectification of the device increases as the gradient segments increases. Here we can explain it in terms of asym-

metric geometry in the MSSG thermal rectifier. In the above simulation with the fixed total length, more gradient segments mean higher geometric asymmetry and therefore greater thermal rectification. Such an MSSG thermal rectifier model is novel, and the enhancement of thermal rectification is encouraging. Therefore, our proposed MSSG thermal rectifier, which is a hierarchical model and can be regarded as a new concept-proof design, will shed some light for the experimental setup or thermal rectifier device design.

3.2.2. Enhancement of thermal rectification by designing multi-segment inhomogeneous porous thermal rectifier

The aforementioned proposed MSSG thermal rectifier is designed based on the exterior shape. Another interesting direction is the design of interior structure. Inhomogeneous geometrical internal structure also has a significant impact on thermal rectification. Next, we will explore the impact of interior structures on thermal rectification. Inspired by nanoporous superlattice,[65] nanoribbon network,[66] porous carbon,[67–69] nanoporous frameworks,[70] and the microstructured cellular biomorphic materials,[71] we will consider pores as tuning factors for the interior structure.

We thus design the multi-segment inhomogeneous porous (MSIP) thermal rectifier. Figure 6 shows the detailed design of the MSIP thermal rectifier, which are generated by creating porous structures inside the segments of the initial geometry of the general multi-segment thermal rectifier, as shown in Fig. 1. We systematically investigate the effects of location, size, and shape of pores on the rectification of the MSIP thermal rectifier.

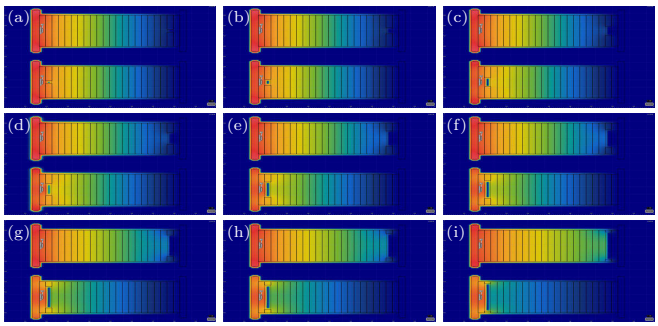


Fig. 6. The multi-segment inhomogeneous porous (MSIP) thermal rectifier. The pores with different relative depths (relative to the thickness of segment) in the second segment are shown from panels (a)–(i): (a) 10% depth, (b) 20% depth, (c) 30% depth, (d) 40% depth, (e) 50% depth, (f) 60% depth, (g) 70% depth, (h) 80% depth, (i) 90% depth.

(I) MSIP thermal rectifier: effects of relative pore depth

The procedure of the setup of the MSIP thermal rectifier is given as follows. The multi-segment thermal rectification model with power source and heat sink, sandwiched with 22 segments (building blocks) is designed as the initial geometry. Then the heat flux sensor and thermometer are placed on the first building block near the hot end. The conductivity of every building block is set to 1 W/(m·K). In order to study the effect of the internal geometrical symmetry on thermal rectification, we create a pore in segments and control the corresponding variables of pore. The variables we test here are the relative thickness, relative width, and relative position of the pore (here the abstract concept method is used to generate the model, and the relative concept can be used for the general cases).

In the simulation, the power density in the power source is adjusted to keep the temperature of first block (the segment with thermometer) to be 60 °C, and the cold end (heat sink) is set to a constant temperature of 0 °C. We create pores in the second building block from the hot end, increasing the relative depth of pore from 10% to 90% in a 10% step of a building block. The thermal rectifications caused by pores with different relative depths are calculated (according to Eq. (4), by the ratio of forward and reverse power densities, similar with the case of MSSG thermal rectifier) and compared with the simulation without pores.

Figure 7 shows the corresponding thermal rectification of MSIP thermal rectifier with pores having different thicknesses. It can be seen that the thermal rectification is higher when the relative thickness of the pore is larger. The thermal rectification increases with the relative thickness of the pore, and the enhancement is significant.

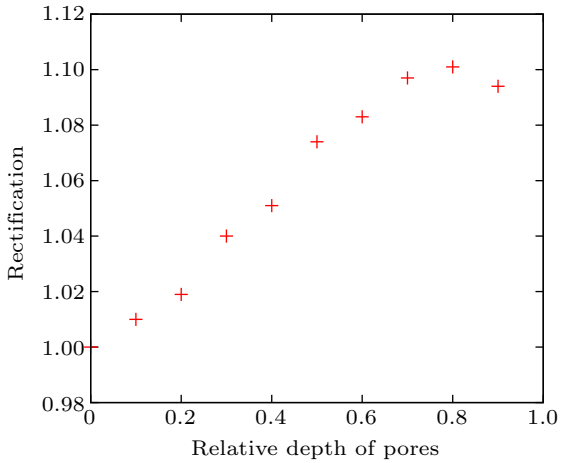


Fig. 7. The rectification of the proposed MSIP thermal rectifier as a function of depth of pores (relative to thickness of segment).

(II) MSIP thermal rectifier: effects of relative pore width

Figure 8 shows the effect of the relative width of the pores on thermal rectification. The heat end is still set to 60 °C, and the cold end is still fixed at a constant temperature of 0 °C. We create pores sequentially from the second building block of the hot end to the 11th building block (the first is for the heat flow meter and thermometer), increasing the relative width from 1/22 to 10/22 in a step of a building block. Then, we calculate the thermal rectification caused by each pore with different relative widths.

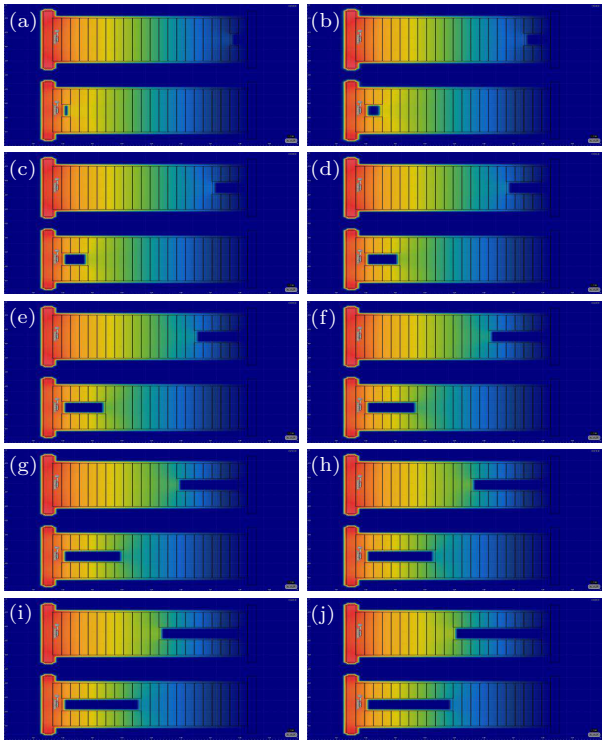


Fig. 8. The MSIP thermal rectifier with the pores having different relative widths (relative to the total width of all segments).

Figure 9 shows the effect of relative thickness on thermal rectification, from which we can see that the relative thickness does not change significantly for thermal rectification (in the range of 1.037–1.043, almost constant compared with thermal rectification vs depth of pores, as shown in Fig. 7).

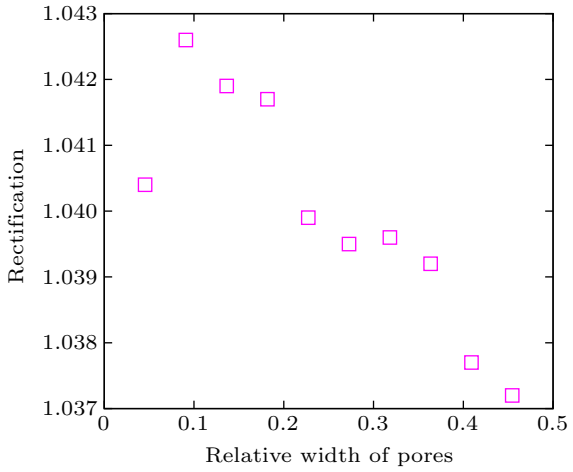


Fig. 9. The rectification of the MSIP thermal rectifier as a function of relative width of pores (relative to the total width of all segments).

(III) MSIP thermal rectifier: effects of relative pore position

Figure 10 shows the effect of the relative position of the pores on thermal rectification. The temperature difference is set to 60 °C. Before proceeding with the location exploration, the pore location is first defined. We use the one end of the entire model as the origin to establish a rectangular coordinate system to determine the position, and the center or middle of the material is defined as 0.5. The pore is located always at the middle of the segment (relative to thickness). Then the relative position of pore can be simplified as the index (i) of the porous segment divided by the total number of segments, *i.e.*, i(pore)/22. Figure 11 shows that the closer the pore is to the endpoint, the greater the thermal rectification.

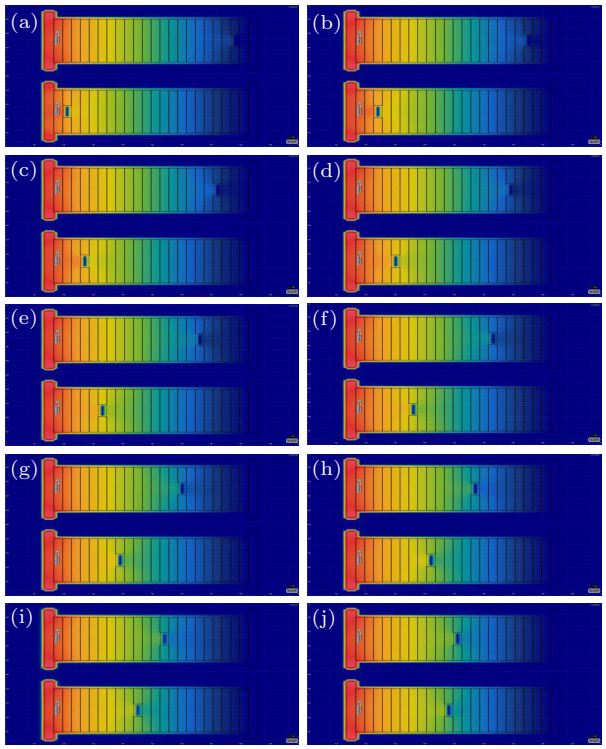


Fig. 10. The MSIP thermal rectifier with the pores at different relative positions (relative to the total width of all segments).

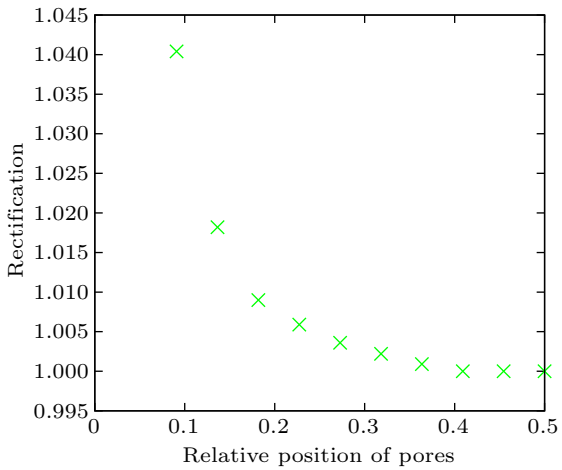


Fig. 11. The rectification of the MSIP thermal rectifier as a function of relative position of pores (relative to the total width of all segments). The cold end in the forward configuration or hot end in the reverse configuration are set to be original point. The middle or center of the material is located at 0.5.

3.3. Enhancement of thermal rectification by combining optimization of thermal conductivity asymmetry and geometric asymmetry

The model by combining thermal conductivity asymmetry and geometry asymmetry is also investigated. Following

the setup for the case of LCO–LSCO bi-segment thermal rectifier (as shown in Fig. 2) but with the increased thermal conductivity asymmetry (Fig. 3), we further enhance the thermal rectification through combining geometric asymmetry by creating pores in the rectifier. The cold end is at constant temperature 40 K, and the first segment at hot end is kept at about 100 K by adjusting the power source. The resulting thermal rectification is then obtained by Eq. (4). The setup and temperature distribution in both different kinds of thermal rectifiers are shown in Fig. 12 for comparison. For the model with thermal conductivity asymmetry only (the parameters are the same as Fig. 3), the thermal rectification is $R = |P_f|/|P_r| = 5.91$. However, for the modified model combining geometry asymmetry, one pore with 75% of size is created in the second segment near the cold end (heat sink) for the "forward" setup, but the same size of pore is located at the second segment near the hot end for the "reverse" setup. The resulting thermal rectification is enhanced to $R = |P_f|/|P_r| = 6.27$. Our simulation clearly demonstrates that combining thermal conductivity asymmetry and geometry asymmetry is a very effective strategy to enhance the thermal rectification.

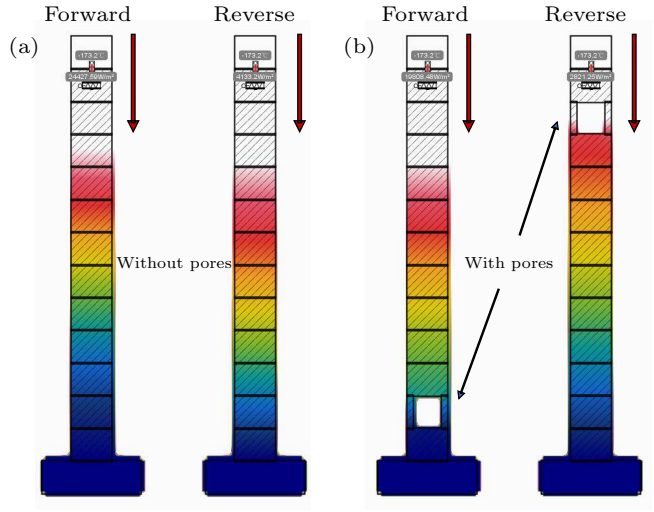


Fig. 12. Multi-stage thermal rectification model combining thermal conductivity asymmetry and geometry asymmetry. The setup is similar with the case of LCO–LSCO bi-segment thermal rectifier, as shown in Fig. 2. The low end is at the constant temperature 40 K, and the first segment at the hot end is kept at about 100 K. (a) Model with thermal conductivity asymmetry only, the same as Fig. 3. The thermal rectification is $R = |P_f|/|P_r| = 5.91$. (b) Model with further geometry asymmetry based on the model in panel (a). One pore with 75% of size is created in the second segment near the cold end (heat sink) for the "forward" setup. In the "reverse" setup, the same size pore is located at the second segment near the hot end. The thermal rectification is increased to $R = |P_f|/|P_r| = 6.27$.

4. Discussion

We have presented the results of thermal rectifiers by three main parts: (i) thermal conductivity effects on thermal rectification, and then (ii) geometric effects on thermal rectification, and finally (iii) the enhancement of thermal rectification through the combined optimization of thermal conductivity asymmetry and geometric asymmetry (namely, usage of results of above (i) and (ii)). Several novel multi-segment thermal rectifiers with various thermal conductivity asymmetry and/or geometric asymmetry as well as with combined design have been proposed.

The physical mechanism behind thermal rectifiers is important to understand the origin of thermal rectification and useful for further improvement of devices. For one-dimensional asymmetric lattice, it has been revealed that the thermal rectification can be induced by nonlinear interactions and nonuniform phonon frequency distribution.[64] It is also found that the energy exchange of the normal mode of vibration induced by asymmetric phonon–phonon interaction may lead to the ballistic thermal rectification.[72] It has also been demonstrated that thermal rectification takes place in asymmetric systems (graded materials)[36,73] with local heat flow proportional to the temperature gradient and with the local conductivity depending on temperature.[73]

For bi-segment thermal rectifiers, the origin of thermal rectification is related to thermal conductivity difference between two segment materials.[35] For the multi-segment thermal rectifiers with asymmetric geometry (either by size gradient or with asymmetric distribution of pores), the mechanism of the thermal rectification enhancement can be explained by the modulation of effective thermal conductivity of asymmetric segment materials. The effective thermal conductivity can be expressed according to Fourier's law,

$$k_{\text{eff}} = \frac{Q/\Delta t}{A(\Delta T/\Delta x)}, \tag{5}$$

where $Q/\Delta t$ is the heat flow rate, ΔT is the temperature gradient applied on segments with length of x, and A is the cross-sectional surface area. When the size of the cross-sectional area is changed, the effective thermal conductivity of the material changes accordingly, resulting in the asymmetry of the effective thermal conductivity, and thus the modulation of thermal rectification.

Most models proposed in this work can be realized in experiments in both the macroscopic scale and the microscopic scale, as long as the Fourier law is still valid within the scale of size. With progress of thermal conductivity in materials in multi-scale[46,74–82] or thin films[83,84] or bulk form,[83–86] the design of efficient thermal rectifiers will have more choices of components. Many advances of characterization[87,88] will be helpful to reveal the microstructures and properties (such as phonon scattering, thermal conductivity, thermal diffusion, thermal capacity, *etc.*), as well as the interface structure[89,90] and interfacial heat transfer[91] of segment materials. Such advanced characterizations combined with thermal rectification measurements can be useful for further study and design of better thermal rectifiers.

5. Conclusion

In this work, we have systematically investigated the multi-segment thermal rectifiers in terms of thermal conductivity asymmetry and geometry asymmetry as well as the effects of combining of both. We proposed the strategies by utilizing the asymmetry engineering approach to enhance the thermal rectification of multi-segment rectifiers. Our simulations demonstrate that increasing the asymmetry of thermal conductivity or the asymmetry of geometry can improve the thermal rectification. Furthermore, combining the asymmetry of both thermal conductivity and geometry, it will have a significant improvement of thermal rectification. The design and asymmetry engineering of multi-segment rectifiers are provided in great details. Our study provides ideas for realizing high thermal rectification in the solid state thermal rectifiers.

Acknowledgments

Project supported by the National Natural Science Foundation of China (Grant No. 12274355) and Xiamen University Malaysia Research Fund (Grant Nos. XMUMRF/2022-C9/IORI/003 and XMUMRF/2022-C10/IORI/004).

References

[1] Kobayashi W, Teraoka Y and Terasaki I 2009 *Appl. Phys. Lett.* **95** 171905
[2] Marucha C, Mucha J and Rafałowicz J 1975 *Phys. Status Solidi A* **31** 269
[3] Marucha C, Mucha J and Rafałowicz J 1976 *Phys. Status Solidi A* **37** K5
[4] Garcia-Garcia K and Alvarez-Quintana J 2014 *Int. J. Therm. Sci.* **81** 76
[5] Hoff H 1985 *Physica A* **131** 449
[6] Sun X, Kotake S, Suzuki Y and Senoo M 2001 *Heat Transfer Asian Res.* **30** 164
[7] Hu B, He D, Yang L and Zhang Y 2006 *Phys. Rev. E* **74** 060201
[8] Dames C 2009 *J. Heat Transfer* **131** 061301
[9] Majumdar A and Reddy P 2004 *Appl. Phys. Lett.* **84** 4768
[10] Starr C 1936 *Physics* **7** 15
[11] Moon J S and Keeler R N 1962 *Int. J. Heat Mass Transfer* **5** 967
[12] Thomas T and Probert S 1970 *Int. J. Heat Mass Transfer* **13** 789
[13] O'callaghan P, Probert S and Jones A 1970 *J. Phys. D* **3** 1352
[14] Chumak K and Martynyak R 2012 *Int. J. Heat Mass Transfer* **55** 5603
[15] Xu W, Zhang G and Li B 2014 *J. Appl. Phys.* **116** 134303
[16] Roberts N and Walker D G 2011 *J. Heat Transfer* **133** 092401
[17] Somers R, Fletcher L and Flack R 1987 *AIAA J.* **25** 620
[18] Barber J and Wright K 1967 *Int. J. Mech. Sci.* **9** 811
[19] Rogers G 1961 *Int. J. Heat Mass Transfer* **2** 150
[20] Powell R, Tye R and Jolliffe B 1962 *Int. J. Heat Mass Transfer* **5** 897
[21] Clausing A 1966 *Int. J. Heat Mass Transfer* **9** 791
[22] Lewis D and Perkins H 1968 *Int. J. Heat Mass Transfer* **11** 1371
[23] Hudson P 1976 *Phys. Status Solidi A* **37** 93
[24] Huang J, Li Q, Zheng Z and Xuan Y 2013 *Int. J. Heat Mass Transfer* **67** 575
[25] Lee J, Varshney V, Roy A K, Ferguson J B and Farmer B L 2012 *Nano Lett.* **12** 3491
[26] Wang L and Li B 2007 *Phys. Rev. Lett.* **99** 177208
[27] Chang C W, Okawa D, Majumdar A and Zettl A 2006 *Science* **314** 1121
[28] Otey C R, Lau W T and Fan S 2010 *Phys. Rev. Lett.* **104** 154301
[29] Casati G 2005 *Chaos* **15** 015120
[30] Li B, Wang L and Casati G 2004 *Phys. Rev. Lett.* **93** 184301
[31] Hu B and Yang L 2005 *Chaos* **15** 015119
[32] Hu B, Yang L and Zhang Y 2006 *Phys. Rev. Lett.* **97** 124302
[33] Peyrard M 2006 *Europhys. Lett.* **76** 49
[34] Hopkins P E and Norris P M 2009 *J. Heat Transfer* **131** 022402
[35] Terraneo M, Peyrard M and Casati G 2002 *Phys. Rev. Lett.* **88** 094302
[36] Yang N, Li N, Wang L and Li B 2007 *Phys. Rev. B* **76** 020301
[37] Toyin O R, Ge W X and Gao L 2021 *Chin. Phys. Lett.* **38** 016801
[38] Hu S Q, An M, Yang N and Li B W 2017 *Small* **13** 1602726
[39] Wehmeyer G, Yabuki T, Monachon C, Wu J and Dames C 2017 *Appl. Phys. Rev.* **4** 041304
[40] Roberts N A and Walker D G 2011 *Int. J. Therm. Sci.* **50** 648
[41] Prstic S, Iyengar M, Arik M, Gektin V, Hodes M, Narasimhan S and Geisler K 2010 *Panel Session at ITherm2010*
[42] Swoboda T, Klinar K, Yalamarthy A S, Kitanovski A and Muñoz Rojo M 2021 *Acta Phys. Sin.* **70** 200625 (in Chinese)
[43] Zhang L M, Jiao B B, Yun S C, Kong Y M, Ku C W and Chen D P 2017 *Chin. Phys. Lett.* **34** 025101
[44] Chi F and Sun L L 2016 *Chin. Phys. Lett.* **33** 117201
[45] Jin Q X, Liu B, Liu Y, Wang W W, Wang H, Xu Z, Gao D, Wang Q, Xia Y Y, Song Z T and Feng S L 2016 *Chin. Phys. Lett.* **33** 98502
[46] Li H L and Cao B Y 2019 *Acta Phys. Sin.* **68** 200201 (in Chinese)
[47] Klinar K, Swoboda T, Muñoz Rojo M and Kitanovski A 2021 *Acta Phys. Sin.* **70** 200623 (in Chinese)
[48] Dietrich M, Euler A and Thummes G 2017 *Cryogenics* **83** 31
[49] Klinar K and Kitanovski A 2020 *Renew. Sust. Energ. Rev.* **118** 109571
[50] Qian S, Yu J and Yan G 2017 *Renew. Sust. Energ. Rev.* **69** 535
[51] Miño-Galaz G A 2015 *J. Phys. Chem. B* **119** 6179
[52] Craven G T, He D and Nitzan A 2018 *Phys. Rev. Lett.* **121** 247704
[53] Sandonas L M, Gutierrez R, Dianat A and Cuniberti G 2015 *RSC Adv.* **5** 54345
[54] Chun W, Ko Y, Lee H, Han H, Kim J and Chen K 2009 *Sol. Energy* **83** 409
[55] Hemaida A, Ghosh A, Sundaram S and Mallick T K 2020 *Sol. Energy* **195** 185
[56] Cui H and Overend M 2019 *Energy Build.* **199** 427
[57] Han C, Chen Z and Li B 2021 *Int. J. Heat Mass Transfer* **179** 121675
[58] Li B, Wang L and Casati G 2006 *Appl. Phys. Lett.* **88** 143501
[59] Wang L and Li B 2008 *Phys. Rev. Lett.* **101** 267203
[60] Tian H, Xie D, Yang Y, Ren T L, Zhang G, Wang Y F, Zhou C J, Peng P G, Wang L G and Liu L T 2012 *Sci. Rep.* **2** 523
[61] Zheng J C 2022 *Research* **2022** 9867639
[62] Xie C 2012 *Phys. Teach.* **50** 237
[63] Klie R F, Zheng J C, Zhu Y, Varela M, Wu J and Leighton C 2007 *Phys. Rev. Lett.* **99** 047203
[64] Zeng N and Wang J S 2008 *Phys. Rev. B* **78** 024305
[65] Fan Z Y, Zheng J S, Wang H Q and Zheng J C 2012 *Nanoscale Res. Lett.* **7** 570
[66] Wang Z Q, Cheng H, Lu T Y, Wang H Q, Feng Y P and Zheng J C 2018 *Phys. Chem. Chem. Phys.* **20** 16510
[67] Wang Y K, Zhang M K, Dai Y, Wang H Q, Zhang H Y, Wang Q Q, Hou W B, Yan H, Li W R and Zheng J C 2019 *J. Power Sources* **438** 227045
[68] Yan H, Wang J H, Fang Y, Zhou M X, Guo X Y, Wang H Q, Dai Y, Li W R and Zheng J C 2019 *Electrochim. Acta* **304** 138
[69] Dai Y, Ma L P, Hu J Q, Wang J H, Yan H, Zhang H Y, Wang H Q, Lai C Y, Li W R and Zheng J C 2021 *Electrochim. Acta* **371** 137792
[70] Sa N, Chong S S, Wang H Q and Zheng J C 2022 *Nanomaterials* **12** 3239
[71] Li X J, Li N, Ren F, Wang K H, Koh C L, Wu M, Wang H Q and Zheng J C 2018 *J. Mater. Sci.* **53** 13955
[72] Ding X and Ming Y 2014 *Chin. Phys. Lett.* **31** 046601
[73] Wang J, Pereira E and Casati G 2012 *Phys. Rev. E* **86** 010101
[74] Wei N, Xu L Q, Wang H Q and Zheng J C 2011 *Nanotechnology* **22** 105705
[75] Zhang Z Q, Qian S, Wang R J and Zhu Z F 2019 *Acta Phys. Sin.* **68** 054401 (in Chinese)
[76] Zhang P P, Tan S H, Peng X F and Long M Q 2020 *Chin. Phys. B* **29** 106801
[77] Wang Q L, Chen Y Y, Aiyiti A, Zheng M R, Li N B and Xu X F 2020 *Chin. Phys. B* **29** 084402
[78] Pan D K, Zong Z C and Yang N 2022 *Acta Phys. Sin.* **71** 086302 (in Chinese)

[79] Wei N, Chen Y, Cai K, Zhang Y Y, Pei Q X, Zheng J C, Mai Y W and Zhao J H 2022 *Green Energy Environ.* **7** 86

[80] Wei N, Chen Y, Cai K, Zhao J, Wang H Q and Zheng J C 2016 *Carbon* **104** 203

[81] Xu L Q, Wei N, Zheng Y P, Fan Z Y, Wang H Q and Zheng J C 2012 *J. Mater. Chem.* **22** 1435

[82] Li C Y, Lin S M, Dai H Y and Lu D L 2018 *Acta Phys. Sin.* **67** 214401 (in Chinese)

[83] Yang S S, Hou Y and Zhu L L 2019 *Chin. Phys. B* **28** 086501

[84] Zhang Y Y, Cheng R, Ni D, Tian M, Lu J W and Zhao Y 2019 *Chin. Phys. B* **28** 078105

[85] Xing H, Wang H Q, Song T, Li C, Dai Y, Fu G, Kang J and Zheng J C 2023 *Chin. Phys. B* **32** 064210

[86] Zhang L, Li N, Wang H Q, Zhang Y F, Ren F, Liao X X, Li Y P, Wang X D, Huang Z, Dai Y, Yan H and Zheng J C 2017 *Chin. Phys. B* **26** 016602

[87] Zheng J C, Zhang L, Kretinin A V, Morozov S V, Wang Y B, Wang T, Li X J, Ren F, Zhang J Y, Lu C Y, Chen J C, Lu M, Wang H Q, Geim A K and Novoselov K S 2016 *2D Mater.* **3** 011004

[88] Zheng J and Wang H 2021 *Sci. Sin-Phys. Mech. Astron* **51** 030007

[89] Wang H Q, Xu J Y, Lin X Y, Li Y P, Kang J Y and Zheng J C 2021 *Light Sci. Appl.* **10** 153

[90] Zhou H, Wu L J, Wang H Q, Zheng J C, Zhang L H, Kisslinger K, Li Y P, Wang Z Q, Cheng H, Ke S M, Li Y, Kang J Y and Zhu Y M 2017 *Nat. Commun.* **8** 1474

[91] Chen Y, Zhang Y Y, Cai K, Jiang J W, Zheng J C, Zhao J H and Wei N 2017 *Carbon* **117** 399